JACS
JOURNAL OF THE AMERICAN CHEMICAL SOCIETY
pubs.acs.org/JACS
Article

Correlated Local Fluctuations in the Hydrogen Bond Network of Liquid Water

Yonghwan Yun, Rustam Z. Khaliullin, and Yousung Jung*

Cite This: J. Am. Chem. Soc. 2022, 144, 13127−13136
Read Online
ACCESS | Metrics & More | Article Recommendations | Supporting Information

ABSTRACT: The hypothesis that liquid water can separate into two phases in the supercooled state has been supported by recent experimental and theoretical studies. However, whether such structural inhomogeneity extends to ambient conditions is under intense debate. Due to the dynamic nature of the hydrogen bond network of liquid water, exploring its structure requires detailed insight into the collective motion of neighboring water molecules, a missing link that has not been examined so far. Here, highly sensitive quantum mechanical calculations detect that the time evolution of nearby hydrogen bonds is strongly correlated, revealing a direct mechanism for the appearance of short-range structural fluctuations in the hydrogen bond network of liquid water for the first time.

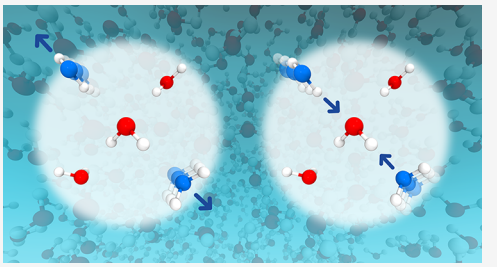

This correlated dynamics is found to be closely connected to the static structural picture. The distortions from the tetrahedral structure do not occur independently but are correlated due to the preference of nearby donors and acceptors to be in similar environments. The existence of such cooperative fluctuations is further supported by the temperature dependence of the local structural evolution and explained by conventional analysis of localized orbitals. It was found that such correlated structural fluctuations are only observed on a short length scale in simulations at ambient conditions. The correlations of the nearby hydrogen bond pairs of liquid water unveiled here are expected to offer a new insight into connecting the dynamics of individual water molecules and the local structure of the hydrogen bond network.

INTRODUCTION

Liquid water, unlike most other liquids, exhibits anomalous behavior of many macroscopic properties such as the density maximum at 4 °C, decreased viscosity under pressure, high surface tension, and the volume expansion on freezing, among many others. These phenomena are believed to arise from the ability of a water molecule to form four strong hydrogen bonds (HBs),[1] exemplified by the ideal solid-state structure of hexagonal water ice.[2] The structure of liquid water has thus long been accepted as a near-tetrahedral configuration with a continuous distribution through the thermal motions.[3−7] Since the finding of the divergence in response functions such as isothermal compressibility and heat capacity upon supercooling,[8,9] the coexistence of two classes of HB environments referred to as low-density liquid (LDL) and high-density liquid (HDL) and the transition between them have been suggested to explain the origin of water's anomalous properties.[8−10] Recent computational and experimental studies have presented evidence of a liquid−liquid phase transition (LLPT) and an associated critical point occurring in the supercooled region.[11−19] The transition between the two local structures has also been suggested to extend to ambient conditions,[9,13,14,20] where the two classes of local structures are referred to as tetrahedral and distorted,[9,13] or symmetrical and asymmetrical structures[5,6] in the literature, in addition to LDL and HDL postulated in the supercooled region. However, this inhomogeneous interpretation of room-temperature water differs from the conventional near-tetrahedral model of water with a continuous distribution and has been debated.[4,21−24]

Due to the constant thermal motions of water molecules and their structural fluctuations generally involving multiple molecules,[25] to fully understand the structure of liquid water it is essential to understand the effect of "collective dynamics" of neighboring water molecules. However, such a link between the collective dynamics and the structure of water has not been made so far. It has been proposed that what makes the water properties unique may arise from its cooperative effect,[26,27] a fundamental property of HB in water whose local HB strength is modified by the presence of other molecules. The cooperativity concept itself has been confirmed in multiple experimental and theoretical cases, but mostly demonstrated in the gas-phase water clusters as a model system.[28−34] Considering the condensed phase nature of liquid water, however, it is highly conceivable for such cooperative effects to play an even more important role in the dynamical behavior of the HB network of room-temperature liquid water. We further

Received: March 2, 2022
Published: July 12, 2022

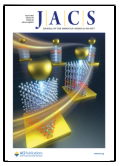

https://doi.org/10.1021/jacs.2c02362
J. Am. Chem. Soc. 2022, 144, 13127−13136

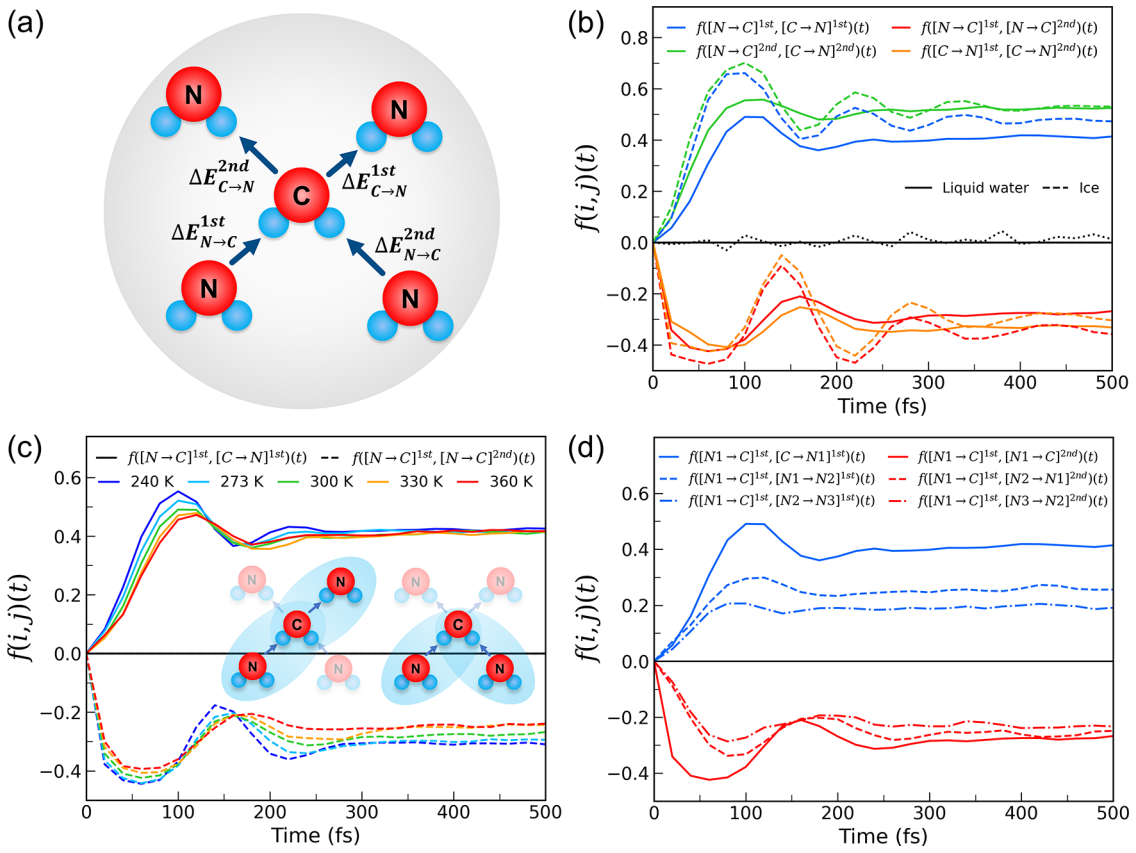

Figure 1. (a) Schematic representation of the first coordination shell neighbors (labeled N) around the central water molecule (labeled C). The arrows indicate the direction of a typical CT and the energy stabilization due to the CT. The superscripts first and second refer to the strongest and second strongest CT interactions as a donor or an acceptor determined at $t = 0$. (b) Evolution of a time-dependent cross-correlation function (TCCF) between two pairs of water in the first coordination shell for liquid water (solid lines) and hexagonal ice (dashed lines). The dotted line in black denotes the TCCF of randomly selected i, j water pairs for comparison. (c) Temperature dependence of two representative TCCFs as illustrated in the inset. (d) Comparison of TCCF within the first coordination shell (C and N1) as shown in (c) (solid lines) vs first and second coordination shell (dashed lines) vs first and third coordination shell (dashed dot lines, see Figure 2 for details) of liquid water.

note that the HB cooperativity is shown to be of particular importance in describing the LLPT at deeply supercooled conditions using the microscopic cell models of water.[11]

We here report the first quantum chemical evidence that local fluctuations in the structure of liquid water are not random but highly correlated due to the underlying cooperativity between the bonds. The correlations are detected and assessed quantitatively using a quantum energy decomposition analysis known as ALMO EDA (absolutely localized molecular orbitals energy decomposition analysis)[35] by measuring the electron density transfer between neighboring molecules, which is remarkably sensitive to their relative positions and orientations (see Methods for details). EDA results demonstrate that the structural fluctuation of liquid water occurs collectively with neighboring molecules correlated in such a way that donor and acceptor have similar structural environments. However, such correlated structural fluctuations are only observed in a small region within the radius of ~6 Å spheres in our ambient simulations. In addition to ALMO EDA, conventional Wannier localized orbitals[36] are utilized to further understand the electronic origin of the correlated dynamics of nearby HBs. Our conclusions are further validated by several other widely used water models at ambient conditions.

RESULTS AND DISCUSSION

Dynamic Correlations between Nearby Hydrogen Bonds. To analyze in detail how the thermal perturbation of a given molecule is linked to the motion of the other molecules, we introduce a time-dependent cross-correlation function (TCCF) for two pairs of water molecules:

$$f(i,j)(t) = \frac{\langle \delta\Delta E_i(t)\cdot\delta\Delta E_j(t)\rangle}{\langle |\delta\Delta E_i(t)|\cdot|\delta\Delta E_j(t)|\rangle} \quad (1)$$

where ΔE_i is the energy stabilization of the ith water pair due to the charge transfer (CT, refer to the Methods section for more details) and $\delta\Delta E_i(t) = \Delta E_i(t) - \Delta E_i(0)$ is the change in the CT energy of the ith pair in the time interval t; the angular brackets denote the ensemble average over all time origins. Thus, $f(i,j)(t)$ measures whether the electron density transfer between two pairs of water molecules (such as two HB pairs) is correlated or anticorrelated in time. In correlated pairs, the CT interactions evolve in the same direction, whereas in anticorrelated pairs the CT energies change in the opposite direction. The extent of correlation between two different ith and jth water pairs is normalized by the absolute value of the change in the CT energy in time interval t. To compute $f(i,j)(t)$, ALMO EDA was performed using snapshots generated in *ab initio* molecular dynamics simulation (AIMD) employing

https://doi.org/10.1021/jacs.2c02362
J. Am. Chem. Soc. 2022, 144, 13127−13136

the BLYP-D3 exchange−correlation functional (see the Methods section for details).

Figure 1a schematically represents the local environment considered in the TCCF with the definitions of associated CT terms around a given ("central") molecule. In Figure 1 and throughout this paper, C stands for the central water molecule and N designates water molecules in the first coordination shell. The superscripts first and second refer to the strongest and second strongest CT interactions as a donor or as an acceptor. It is worth noting that, in this work, the terms donor and acceptor refer to electron donors and electron acceptors, which is opposite the usual description of hydrogen bonding with hydrogen donors and acceptors. In the calculations of TCCF, we use the two strongest donors and two strongest acceptors around the given (central) water molecules based on the magnitude of the CT terms. Since the initially determined configurations of liquid water are constantly fluctuating, for a chosen molecule these two strongest CT donors and acceptors may change as the system evolves. Thus, we only consider the water molecules whose two strongest donors and acceptors remain "intact" during the investigated time interval (∼500 fs), which is noticeably shorter than the average lifetime of an HB (1.4 ps).[37] The two strongest CT donors and acceptors are regarded as intact if their strengths determined at $t = 0$ remain the first or second strongest CT energies at time t. Approximately 60−80% of the initially determined CT pairs remain "intact" after 500 fs (Figure S1).

As the results are summarized in Figure 1b, notably, two types of relative intermolecular motions (correlated vs anticorrelated) are clearly identified by the different signs of the TCCF. The charge flow of donor and acceptor mostly evolves in the same way (correlated), whereas the charge flow of two acceptors (or two donors) mostly evolves in the opposite way (anticorrelated), as characterized by the positive and negative values of the TCCF, respectively. These two opposite signs of correlations within the first coordination shell are significant when compared to the TCCF of randomly selected i, j water pairs (dotted line in black), indicative of the stochastic fluctuations. These correlated motions are also related to the nonadditive binding energy calculations in water clusters; two acceptors (or two donors) were predicted to be repulsive to each other since the three-body term destabilizes the overall binding energy in the water cluster calculations.[28,29,32] Comparison with ice reveals that these correlated fluctuations are indeed an intrinsic property of the condensed phase water, in both liquid water and ice. It is worth mentioning that the changes in the CT energy in eq 1 are directly linked to changes in the relative position of nearby water molecules. It is known that the CT energy decreases exponentially with an increase in the intermolecular distance due to the connection of the former to the orbital overlap.[35] Therefore, it is reasonable to assume that the stretching of HBs affects the CT terms strongly, while intermolecular rotations that break HBs might also play a role. The degree of these correlated and anticorrelated motions gradually increases with decreasing temperature (Figure 1c). In other words, the motion of water molecules becomes more correlated as the random thermal effect is reduced. In addition, these correlated and anticorrelated HB dynamics extend beyond the first coordination shell (Figure 1d), at least up to the third coordination shell as calculated here, though the extent of correlations in HBs is reduced as the distance between molecules increases compared to the HBs within the first coordination shell.

The Link between Dynamic Correlation and the Statistical Structural Picture. To reveal how these correlated dynamics couple to the statistical structural picture, we first consider the correlation in the joint distribution of CT energies for two pairs with the same order of strength in the first coordination shell of the given central molecule. The joint distributions in CT energy between donor and acceptor are plotted in Figure S2, and their Pearson correlation coefficients are summarized in an inset table in Figure 2.

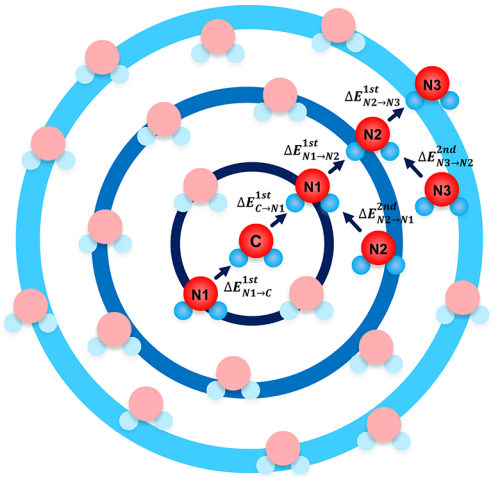

Two CT pairs	1st shell		2nd shell	3rd shell
	$\Delta E^{1st}_{N1\to C}, \Delta E^{1st}_{C\to N1}$	$\Delta E^{2nd}_{N1\to C}, \Delta E^{2nd}_{C\to N1}$	$\Delta E^{1st}_{N1\to C}, \Delta E^{1st}_{N1\to N2}$	$\Delta E^{1st}_{N1\to C}, \Delta E^{1st}_{N2\to N3}$
Liquid water	0.27	0.35	0.05	0.01
Ice	0.22	0.22	0.04	0.01

Figure 2. Pearson correlation coefficients between the donor CT energies and the acceptor CT energies as a function of coordination shell (actual two-dimensional joint distributions are shown in Figure S2). Shown in the upper panel is the schematic representation of the first, second, and third coordination shell molecules (labeled N1, N2, and N3) around the central water molecule (labeled C). In $\Delta E_{N\to C}$ or $\Delta E_{C\to N}$, the superscripts first and second refer to the strongest and second strongest CT interactions as a donor or an acceptor. The Pearson correlation coefficients for ice are also shown for comparison.

Although the magnitude is relatively small, positive correlation coefficients between the donor and acceptor CT energies are clear and consistent with the results of correlated dynamics shown in TCCF (Figure 1), suggesting that the dynamic behaviors identified by TCCF are well reflected in the statistical structural pictures. Incidentally, unlike the dynamic correlations that were observed to extend to second and third coordination shells (Figure 1d), statistically and statically, the structural correlations appear mainly at short ranges probably due to the reduced dynamic correlations at longer ranges, seen by the very small or close to zero correlation coefficients in CT energies beyond the first coordination shell. Qualitatively the same statistical correlation pictures are also seen in ice.

To further link the dynamics and structural transition in greater detail, we focused on the correlations between the second strongest donor/acceptor CT energies since they are related to the HB-breaking events. We used an electronic threshold ($\Delta E^{min}_{C\to N} = -4.88$ kJ/mol, see Section 1 in the Supporting Information (SI) for details) to determine whether

https://doi.org/10.1021/jacs.2c02362
J. Am. Chem. Soc. 2022, 144, 13127−13136

an HB is formed or broken. Being sensitive to the relative position and orientation between neighboring molecules, this electronic structure-based definition yields the geometric features that are compatible with the geometry-based HB definitions conventionally employed (Figure S4).

The correlations between the second strongest donor/acceptor CT energies (Figure 3b) are related to the HB-breaking events, as they involve the evolution from the bonding to nonbonding region of donor/acceptor CT energies (the breaking of the donor/acceptor). That is, if one of the second strongest donor HBs is broken with the magnitude of CT energies below the HB threshold (dashed lines in Figure 3b), the second strongest acceptor HB is also likely broken with the magnitude of CT energies below the HB threshold. This can be compared with the case in the strongest donor/acceptor CT energies (Figure 3a) or ice, where the similar dynamic correlations and similar two-dimensional joint distributions in CT energies are observed but with the HB-breaking events rarely occurring due to the CT energies not evolving into the nonbonding region.

To support such structural transitions (fluctuations) further, we calculated the HB autocorrelation function,[37] $c(t)$, for the second strongest donor CT interaction ($\Delta E^{2nd}_{C\to N}$) when the second strongest acceptor CT interaction ($\Delta E^{2nd}_{N\to C}$) remains intact vs when it breaks after time t (see insets in Figure 3c).

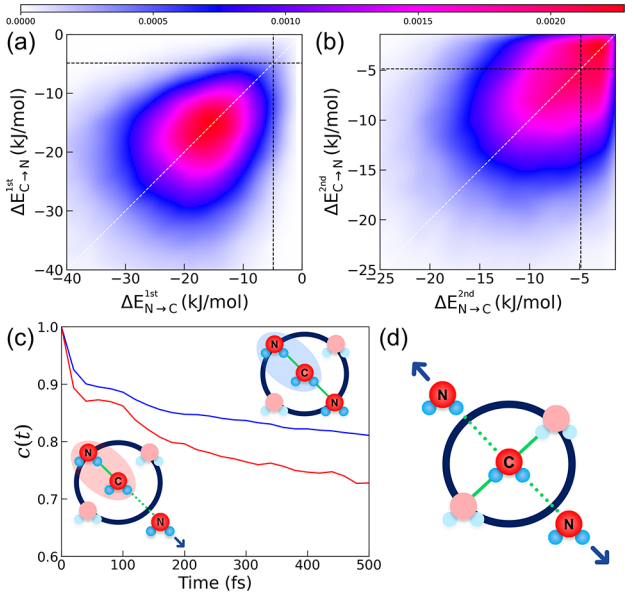

Figure 3. (a, b) Distribution of two CT pairs with the same order of strength of liquid water. The CT energies of acceptor and donor pairs considered in Figure 1b are assigned to the x- and y-axis. The dashed white lines indicate that the two CT energies are the same. The dashed black lines correspond to the CT energy of −4.88 kJ/mol, a threshold to separate bonding and nonbonding configuration (see main text). For $\Delta E^{2nd}_{N\to C}$ and $\Delta E^{2nd}_{C\to N}$ in (b), CT energies stronger than −1.4 kJ/mol are only included to display the distribution clearly. Also, see Figure 2 for the Pearson correlation coefficients corresponding to these plots. (c) Time-evolution of the HB autocorrelation functions of the second strongest donor CT interaction ($\Delta E^{2nd}_{C\to N}$) when the second strongest acceptor CT interaction ($\Delta E^{2nd}_{N\to C}$) remains intact (blue) and when it breaks (red) after time t, as shown in the insets. (d) Cartoon of correlated structural fluctuation of the second strongest CT interacting pairs.

$$c(t) = \langle h(t)h(0)\rangle / \langle h(0)^2\rangle \quad (2)$$

where $h(t)$ is 1 if the HB exists at a time t while $h(t)$ is 0 if it does not exist at time t.

Figure 3c shows that the survival probability of the second strongest "donor" CT interaction ($\Delta E^{2nd}_{C\to N}$) decays faster when the second strongest "acceptor" interaction ($\Delta E^{2nd}_{N\to C}$) breaks compared to the case when the second strongest "acceptor" interaction remains bonding after time t. Thus, the HB breaking of "donor" molecules is indeed dynamically connected with that of "acceptor" molecules. This correlated structural transition (fluctuation) shown in Figure 3b,c is schematically illustrated in Figure 3d.

Structural Fluctuations in the First Coordination Shell of Liquid Water. To further analyze the structural transition in greater detail, we investigated the strength of the donor HBs depending on the varying number of acceptors. In Figure 4, the joint distribution of the first two strongest donor CT energies for a given central molecule ($\Delta E_{C\to N}$) is plotted depending on the number of acceptors of the chosen central molecule. Figure 4 clearly shows that the two-dimensional distribution of the CT energy of the two strongest donors reveals a markedly different pattern depending on the number of acceptors. The strength of donor CT energies progressively weakens as the number of acceptors decreases. To describe these results quantitatively, the joint distribution of the donor CT energies in each panel is partitioned into three regions: 2-donor (both $\Delta E^{1st}_{C\to N}$ and $\Delta E^{2nd}_{C\to N}$ are stronger than the threshold −4.88 kJ/mol), 1-donor (only one of $\Delta E^{1st}_{C\to N}$ and

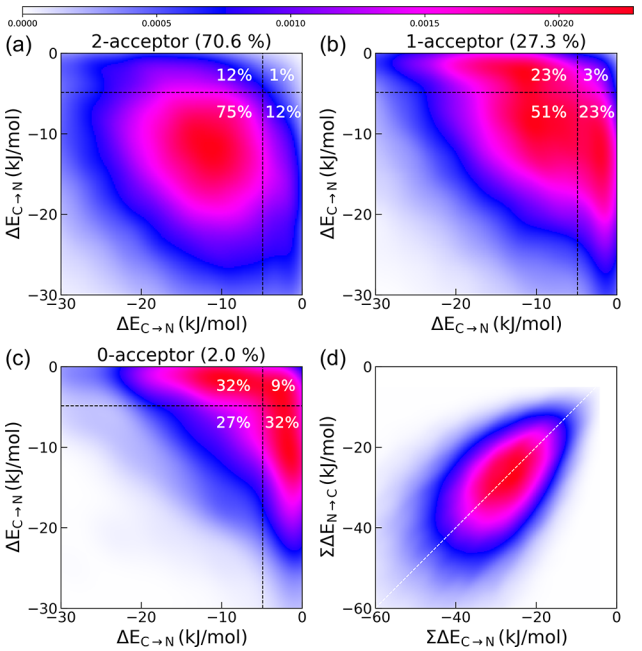

Figure 4. (a−c) Distributions of donor CT (from the central molecule to the first two strongest neighbors) energies for central molecules with 2, 1, and 0 acceptors. Two-donor CT energies ($\Delta E_{C\to N}$) were randomly assigned to the x- or y-axis. The dashed lines correspond to the CT energy of −4.88 kJ/mol, a threshold to count HBs (see main text). The numbers in parentheses denote the percentage of each configuration. The 3-acceptor configuration is negligible (<0.1%) and not shown. (d) Distribution for the sum of all donor CT energies ($\sum\Delta E_{C\to N}$, x-axis) and acceptor CT energies ($\sum\Delta E_{N\to C}$, y-axis).

https://doi.org/10.1021/jacs.2c02362
J. Am. Chem. Soc. 2022, 144, 13127−13136

$\Delta E^{2nd}_{C\to N}$ is stronger than −4.88 kJ/mol), and 0-donor (both $\Delta E^{1st}_{C\to N}$ and $\Delta E^{2nd}_{C\to N}$ are weaker than −4.88 kJ/mol) regions.

Figure 4a shows that when the central molecule has two electron acceptors, it also has a high fraction (75%) of 2-donor configurations. When the number of acceptors is reduced from two to one driven by thermal agitation (Figure 4b), the strength of the donor CT energies decreases. This is most evident on the basis of the appearance of the low-energy peaks in the 1-donor region (from 24% to 46%). In fact, the boundaries in Figure 4b separate two types of peaks in different regions. In addition, the position of the peak in the 2-donor region is shifted from −10.7 to −7.2 kJ/mol. That is, if a tetrahedrally coordinated water molecule (2-acceptor 2-donor configuration) loses one acceptor, the chance of losing one donor partner increases evidently by the emergence of low-energy peaks and by the weakening of a high-energy peak. This reflects that although the majority of water molecules in our model of liquid water have two acceptors (1.69 acceptors per molecule, which is consistent with a recent experimental tetrahedrality of 1.74 ± 2.1% donated and accepted HBs per molecule[7]), indicative of tetrahedral (symmetrical) structure, highly correlated fluctuations cooperatively give rise to a distorted (asymmetrical) structure revealed by one donor and one acceptor configuration.

It is important to note that, in the 1-acceptor configuration (Figure 4b), the two peaks (−11.8 kJ/mol) at the 1-donor region have a stronger CT energy than the peak (−10.7 kJ/mol) at the 2-donor region in 2-acceptor configuration by 1.1 kJ/mol, suggestive of the presence of a "strong HB".[23,34,38] This analysis does not prove or disprove a recently proposed dynamic polymer picture of liquid water,[23,24] but rather indicates that, on the scale of two or three HBs, water molecules with only one donor can have a stronger HB than molecules with two donors on average. This phenomenon is related to the anticorrelation in Figure 1 and agrees with a usual chemical intuition: removing one of the two bonds makes the remaining bond stronger. Despite the low fraction (2.0% in Figure 4c), it should also be noted that the central molecules with the 0-acceptor have considerably weak donor interactions (a peak appearing at −1.3 kJ/mol), which further supports the balanced energy contribution from acceptors and donors and the resulting molecular environments between them. The latter similarity of structural environments between donor and acceptor is also evident from the two-dimensional distribution of the sum of all donor CT energies ($\sum\Delta E_{C\to N}$) and acceptor CT energies ($\sum\Delta E_{N\to C}$) with a Pearson correlation coefficient of 0.55 (Figure 4d). This relationship between donor and acceptor is also consistent with correlated molecular motion in Figure 1. The analyses presented above also hold the same conclusions when performed with the varying number of donors instead of acceptors (Figure S5).

Structural Evolutions as a Function of Temperature. The correlated short-range structural fluctuations presented in Figure 4 are further strengthened by the change in the population of local structures as a function of temperature (Figure 5). The local environment is characterized by the number of electron acceptors (A) and electron donors (D), where the use of electronic (Figure 5a) or geometric (Figure 5b) definitions[39] to count HBs yields qualitatively the same conclusions.

Figure 5 shows that the tetrahedral (2A2D) configuration is the dominant species at all investigated temperatures (240−360 K), and there are some distorted species, in line with the conventional tetrahedral model of liquid water. Previous experimental[12,40] and theoretical[41−43] studies have shown that the four-coordinated tetrahedral motif decreases while the distorted motifs increase in population as the temperature rises. What is interesting to notice here is that structural transitions occur nonuniformly when the population of the tetrahedral structure decreases. The most significant nonuniform structural transformation is from the four-coordinated 2A2D to the 1A1D configuration. That is, when the tetrahedral structure is distorted due to thermal fluctuation, the evolution occurs such that the 1A1D configuration is preferentially formed. This correlated evolution picture becomes obvious when compared to the population changes of other configurations. For example, the 2A0D configuration with the same number of HBs as 1A1D is insensitive to temperature changes. Therefore, donor and acceptor prefer to have similar structural environments, as suggested in the correlated structural behaviors in Figure 4, also consistent with the interpretation of Raman spectroscopy data.[44]

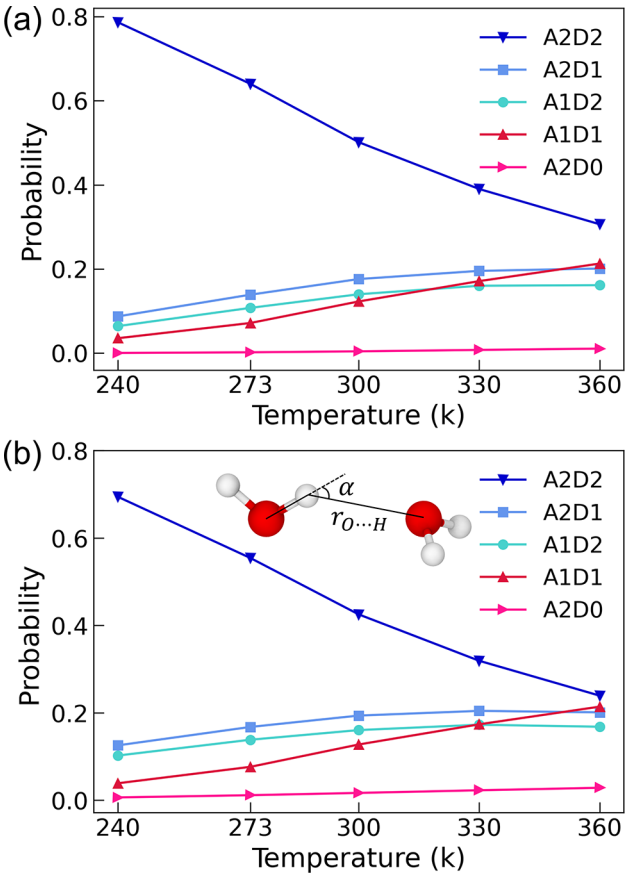

Figure 5. Population of local structures distinguished by the number of neighbors as a function of temperature (240−360 K). A and D stand for electron acceptor and electron donor, respectively, and the numbers to the right of A and D indicate their respective numbers. (a) Electronic threshold (−4.88 kJ/mol) and (b) geometric criteria (1.59 Å < $r_{O\cdots H}$ < 2.27 Å and α < 40°, see the inset) were used to count HBs. While only five major configurations are shown here for clarity, the entire population of all possible configurations at different temperatures is shown in Figure S6.

Analysis of the Structural Heterogeneity in Liquid Water. In addition to the two-dimensional distributions in Figure 4, Figure 6a shows a one-dimensional distribution for two donor CT energies without the decomposition relying on

https://doi.org/10.1021/jacs.2c02362
J. Am. Chem. Soc. 2022, 144, 13127−13136

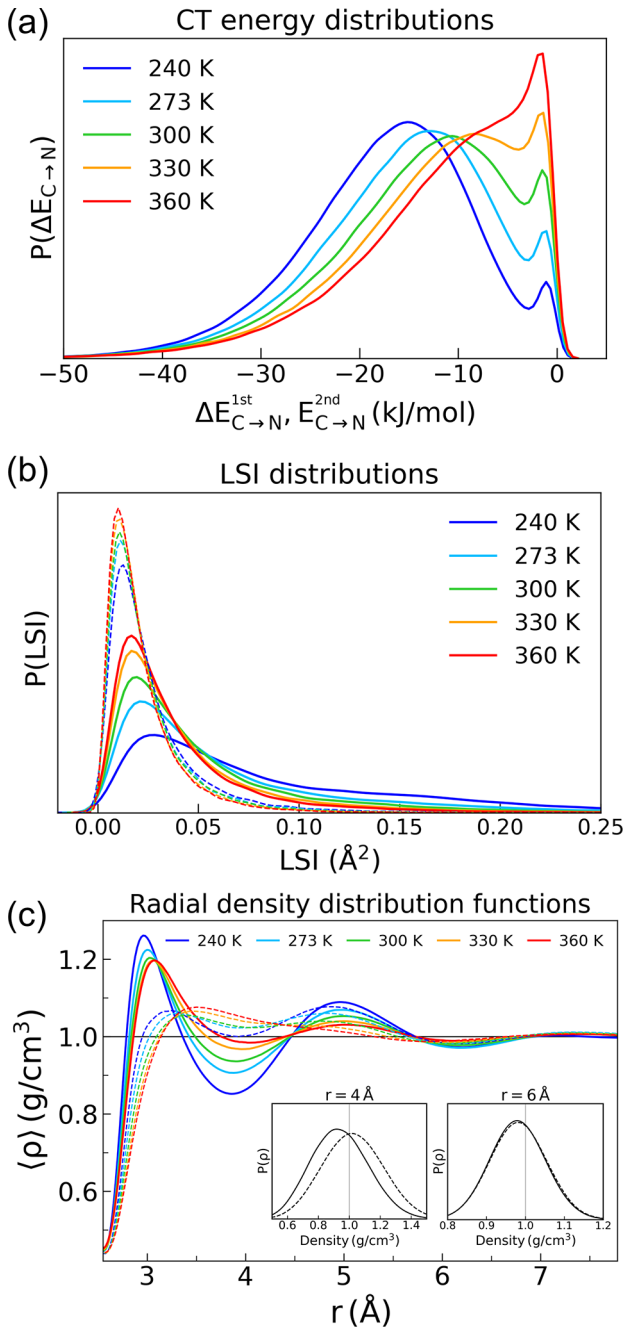

Figure 6. (a) One-dimensional probability density distributions of two electron donor CT energies ($\Delta E^{1st}_{C\to N}$, $\Delta E^{2nd}_{C\to N}$) at different temperatures. (b) Probability density distributions of the local structure index (LSI) parameter of tetrahedral (solid lines) and distorted (dashed lines) structures at different temperatures. (c) Spherically averaged local density of tetrahedral (solid lines) and distorted (dashed lines) water configurations as a function of distance at different temperatures. The local density distributions using a sphere of a fixed radius of 4 and 6 Å at 300 K are shown in insets.

the number of acceptors. The two strongest interactions are selected since their strengths are mainly responsible for the structure of liquid water. High- and low-energy peaks are seen in a wide range of temperatures (240−360 K), which indicates intact and broken HBs. The relative area and height of the low-energy peak (broken HBs) increase with temperature. We note that the presence of two CT energy peaks revealed in Figure 6a refers to the existence of two kinds of CT "pairs" (intact vs broken HBs), but is not an indication of two types of "local structures" such as tetrahedral and distorted,[9,13] or LDL and HDL structures observed in supercooled water.[8,14,18,19]

To detect any sign of structural inhomogeneity, the local configurations in Figure 5 were classified into tetrahedral with 4HBs and distorted with one or more broken HB structures. The local structure index (LSI)[45,46] is utilized to distinguish the two structural motifs geometrically. The LSI offers a quantitative estimate of the local inhomogeneity as an order parameter (see Methods for details) and has been employed to characterize the LDL- and HDL-like environments.[41,47,48] We decomposed the LSI analysis into the contributions from tetrahedral structures and those from distorted structures. Figure 6b shows that the distorted structure with interstitial molecules leads to slightly lower LSI values than those of the tetrahedral structure. However, the difference in LSI values between the two local structures is rather small, and LSI distributions do not show the distinctive bimodal LSI distribution obtained from the inherent structure (quenched 0 K) and interpreted to support the presence of two separate states.[47,48] It is important to note that the spatial size of the structurally correlated regions has not been established reliably, partially due to the presence of a rather arbitrary parameter in the LSI (3.7 Å distance cutoff, see Methods for details). To eliminate this ambiguity, we calculated another order parameter—the radial density distribution function (RDDF)—for the two structural motifs, tetrahedral and distorted, by counting oxygen atoms around water molecules in tetrahedral and distorted water configurations within the spheres of varying radius (Figure 6c). This parameter-free spatially averaged structural property not only characterizes the difference in the two classified structures in the context of HDL and LDL but also reveals the spatial extent of two distinct local environments in liquid water. In essence, this RDDF conveys similar insights to the conventional radial distribution function (RDF, Figure S8), but instead of the spherical shell considered in RDF, RDDF considers the spherical volume and calculates the average local density around the given central water molecule.

As shown in Figure 6c, the RDDFs for tetrahedral and distorted structures deviate, but only in a relatively small radius of 6 Å for all temperatures studied at ambient conditions. In insets of Figure 6c, we also plotted the actual distribution of local density using the sphere of a fixed radius of 4 Å around the tetrahedral (solid lines) and distorted (dashed lines) environments. The peak of the distribution around the tetrahedral structures appears at a slightly lower density than that for the distorted structures, reminiscent of the LDL-like and HDL-like water structures, respectively. This difference in density between the tetrahedral and distorted structures, however, disappears when the local density is evaluated using a larger spherical volume with a radius of 6 Å. This observation that the structural correlation length is around 6 Å in radius, coupled with the fast dissipation of the molecular correlations after a few HBs (inset table in Figure 2), suggests that the signatures of LDL-like and HDL-like structures only show up in a small microscopic length scale, and the structural heterogeneity in an extended length scale is not evident in our simulations and analyses.

Wannier Orbitals of Water Molecules. The maximally localized Wannier functions (MLWFs)[36] are employed to understand the observed correlated behaviors in terms of molecular polarizability. The MLWFs represent the electronic

https://doi.org/10.1021/jacs.2c02362
J. Am. Chem. Soc. 2022, 144, 13127−13136

structure using the localized functions in real space obtained by the unitary transformation of the Kohn−Sham orbitals. The unique feature of MLWFs offers a chemically intuitive means to monitor how the investigated molecule is polarized by the electric field of the surrounding water molecules by conveniently measuring the displacement of their centers. The overall MLWFs are decomposed into contributions from different local environments, distinguished by the number of electron acceptors around the central molecule. We analyzed in Figure 7a the distributions of the distance between oxygen

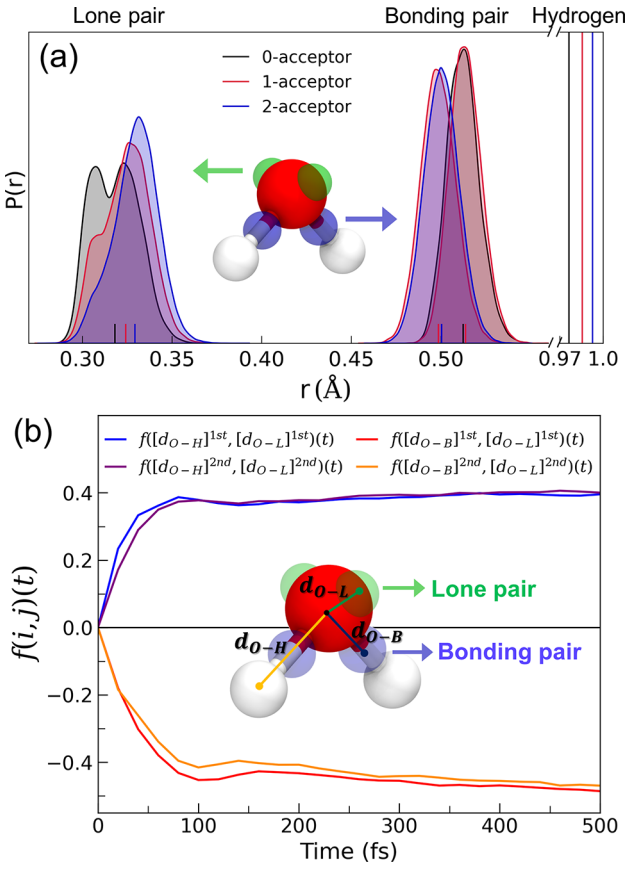

Figure 7. MLWFs of water molecules. (a) Probability distributions of the distances between oxygen and the centers of four MLWFs decomposed by the number of acceptors denoted as 0-, 1-, and 2-acceptor. The small vertical bars on the *x*-axis indicate the average value of each distribution. For 1-acceptor configurations, the HB and non-HB pairs of the MLWF centers are further distinguished as separate probability distributions. The vertical lines on the right indicate the average length of the covalent O−H bond in each configuration. The inset illustrates a representative snapshot of the lone (green) and bonding (blue) electron pairs of a water molecule. (b) TCCF between the center of Wannier orbitals and between the lone pair and the covalent OH bond in a water molecule. d_{O-L}, d_{O-B}, and d_{O-H} refer to the distance from the oxygen atom to the lone pair, bonding pair, and hydrogen atom, respectively. 1st and 2nd refer to the strongest and second strongest interacting pair based on the distance from oxygen.

nuclei and centers of the four MLWFs. The two regions of peaks correspond to the bonding electron pairs located along the O−H bonds occurring at larger distances and the lone electron pairs at shorter distances.

In Figure 7a, the distance between oxygen and lone pair electrons increases progressively as the number of acceptors increases. This elongated lone electron pair with the increasing number of acceptors yields a more negative electric environment, leading to the interaction of the central oxygen with the surrounding hydrogens being more facile. On the contrary, the distance between oxygen and bonding MLWF centers decreases with the increasing number of acceptors from 0 to 2. This trend is opposite to the changes in the length of the covalent O−H bond.[49] Interestingly, however, water molecules with 1-acceptor show one strong (even stronger than that of 2-acceptor configurations) and one weak (even weaker than that of 0-acceptor configurations) HBs. This fact reflects an intramolecular charge transfer from bonding hydrogen to nonbonding hydrogen as suggested by Wernet et al.[38] for 1-acceptor configurations. Therefore, hydrogen atoms that do not take part in the HB are more electronegative and retain a lower ability to form an HB with other molecules. It can also be seen that the pronounced shoulder on the lone pair peak of the 1-acceptor suggests the highly increased number of broken donor interactions, in line with Figure 4b. The qualitatively same results are observed when the analysis is performed as a function of the number of donors (Figure S9). To analyze the dynamic correlation of Wannier orbitals, we calculated the time-dependent cross-correlation function in eq 1 for Wannier orbitals, where we used the displacement of Wannier orbitals $\delta d_{O-X}(t) = d_{O-X}(t) - d_{O-X}(0)$ (X refers to the centers of four MLWFs) and covalent OH bond $\delta d_{O-H}(t) = d_{O-H}(t) - d_{O-H}(0)$ in the same manner as the CT energetics. Figure 7b shows that the time evolution of negative electron pairs and positive nuclei (hydrogen atoms) with respect to the oxygen atom is also correlated. The direction of charge flow within a molecule is consistent with static results (Figure 7a); that is, hydrogen atoms lose electrons to the oxygens.

Validation with Other Water Models. To verify that our conclusion on the correlated structural fluctuations in liquid water is not limited to the water model used in this work, we applied the same analysis to the snapshots generated in molecular dynamics simulations relying on various other water models (MB-pol,[50] SPC/E,[51] TIP4P/2005[52]). The same conclusion is indeed drawn from other water models (Figures S10 and S11), making our findings independent of simulation details. Among them, we note that MB-pol, which can describe polarizability and many-body effects by using large sets of high-level quantum chemical data for up to trimers,[41,50] has been shown to reproduce well various properties of water better than several DFT models even when Hartree−Fock exchange was added to the functional.[53] The MB-pol trajectory-based results, in particular, were almost the same (Figures S11 and S12) as the BLYP-D3 results. Comparison with other water models also shows that the degree of correlations decreases in the classical force field with fixed charge (SPC/E, TIP4P/2005). This comparative analysis highlights the crucial role of polarizability and many-body effects in describing dynamic correlations and structural fluctuations.

CONCLUSIONS

In summary, a highly geometry-sensitive energy decomposition reveals the first electronic structure evidence of correlated local fluctuations in the hydrogen bond network of liquid water arising due to the underlying cooperative nature of intermolecular interactions. In particular, the distortions from the tetrahedral structure are not random but are strongly correlated because of the preference of nearby HB donors and acceptors to be in similar environments. Nonuniform structural

https://doi.org/10.1021/jacs.2c02362
J. Am. Chem. Soc. 2022, 144, 13127−13136

changes as a function of temperature also support this conclusion of directed structural transformation. However, in ambient conditions, these correlations of neighboring HBs rapidly dissipate after a few HBs, and thus two fluctuating structures do not develop on a large length scale in our simulations. Our results raise the question of whether it is possible that the structural fluctuations described in this work contribute to the development of the two phases of supercooled water and the transition between them. The microscopic understanding of locally correlated HBs presented in this work is expected to offer deeper insight into controversies that still exist around the structure and dynamics of liquid water and thereby provide a new perspective to explain several anomalous macroscopic properties of water.

METHODS

***Ab Initio* Molecular Dynamics.** *Ab initio* molecular dynamics simulations of a periodic cell were performed at constant temperature and density for liquid water (128 water molecules at 300 K) and hexagonal ice (96 water molecules at 268 K). The initial configuration for liquid water was obtained from an equilibrated structure from classical MD simulations at 300 K. After 120 ps of equilibration in the NVT ensemble at 330 K, additional 120 ps NVT simulations were performed at different temperatures for the production run. The last 70 ps AIMD trajectory was used for dynamic analysis, and 90 ps was used for static analysis out of a 120 ps NVT run at all investigated temperatures. Due to the longer structural relaxation times at low temperatures, we ran an additional 50 ps at 240 and 273 K for equilibration and further validated aspects of equilibration at lower temperatures (see Section 3 in the SI for details). A short time step of 0.5 fs ensured accurate integration of the equations of motion. The temperature was controlled by the canonical-sampling velocity-rescaling thermostat.[54] In the dual Gaussian and plane-wave scheme implemented in CP2K,[55] a triple-ζ Gaussian basis set with two sets of polarization functions (TZV2P)[56] was used to represent molecular orbitals, and a plane-wave cutoff of 400 Ry was used to represent the electron density. Separable norm-conserving Goedecker−Teter−Hutter pseudopotentials were used to describe the interactions between the valence electrons and ionic cores,[57,58] and the Brillouin zone was sampled at the Γ-point. The exchange−correlation energy was approximated with the BLYP[59,60] functional with the D3 dispersion correction of Grimme.[61]

Energy-Decomposition Analysis. The strength of the individual HBs in liquid water is described by the energy stabilization due to the CT obtained from ALMO-EDA.[35] ALMO EDA decomposes the total intermolecular binding energy (ΔE_{TOT}) into the frozen-density energy (ΔE_{FRZ}), intramolecular polarization energy (ΔE_{POL}), and charge-transfer energy (ΔE_{CT}) and a generally small higher-order (ΔE_{HO}) relaxation term (see ref 35 for a detailed description of the ALMO EDA terms).

$$\Delta E_{TOT} = \Delta E_{FRZ} + \Delta E_{POL} + \Delta E_{CT} + \Delta E_{HO} \tag{3}$$

$$\Delta E_{CT} = \sum_{A,D=1}^{Mol} \Delta E_{D\rightarrow A} \tag{4}$$

Like all other EDA methods based on density functional theory, ALMO EDA does not provide a well-defined recipe to separate the frozen-density and polarization terms into molecular contributions (e.g., single-molecule, two-body terms). While these terms contribute to the overall stabilization of the HB network, this work focuses on the CT energies that can be readily decomposed into pairwise contributions as shown in eq 4.[35] A two-body CT term $\Delta E_{D\rightarrow A}$ corresponds to the orbital relaxation arising from the charge transfer from the occupied orbitals of electron-donor molecule D to the virtual orbitals of electron-acceptor molecule A. A deep connection between the CT terms and various properties of water has been pointed out in several recent articles.[62−68] Since quantum chemical calculations have suggested the CT (electron delocalization) is responsible for the cooperativity (nonadditivity),[30,31] the ALMO EDA provides one of the direct means of probing and estimating the degree of cooperativity of liquid water. ALMO EDA for liquid water was performed using the CP2K package[55] for 901 equidistant snapshots (i.e., configurations of 115 328) separated by 100 fs for static analysis and 3501 equidistant snapshots (i.e., configurations of 448 128) separated by 20 fs for dynamic analysis. CP2K employed the mixed Gaussian and plane-wave approach,[55] which is ideal for ALMO EDA because the localized atom-centered Gaussian basis sets are required for the construction of absolutely localized molecular orbitals, while plane waves are used to represent the charge density for computational efficiency. Molecular orbitals in all ALMO EDA calculations were represented by a triple-ζ Gaussian basis set with two sets of polarization functions (TZV2P).[56] A high-energy cutoff of 1000 Ry was used to describe the electron density. Separable norm-conserving Goedecker−Teter−Hutter pseudopotentials were used to describe the interactions between the valence electrons and ionic cores,[57,58] and the Brillouin zone was sampled at the Γ-point. The exchange−correlation energy was approximated with the BLYP functional.[59,60] We verified that performing ALMO EDA with other density functionals (PBE, SCAN, PBE0) does not affect the main conclusion of this work (see Section 4 in the SI for details).

Local Structure Index. The LSI is an order parameter to quantify the extent of the structural ordering of molecules around the first and second coordination shells.[45,46] The LSI is defined as

$$\mathrm{LSI} = \frac{1}{N}\sum_{i=1}^{N}[\Delta_{i+1,i} - \langle\Delta\rangle]^2 \tag{5}$$

where $\langle\Delta\rangle$ is the mean of differences in distance, $\Delta_{i+1,i} = r_{i+1} - r_i$, between consecutive oxygen atoms around a given molecule $r_1 < r_2 < \cdots < r_i < r_{i+1} < \cdots < r_N < 3.7$ Å $< r_{N+1}$ where N is the number of oxygen atoms that are within 3.7 Å from molecule i. Thus, the LSI provides a quantitative measure of the local structural environment surrounding a given water molecule.

ASSOCIATED CONTENT

Supporting Information

The Supporting Information is available free of charge at https://pubs.acs.org/doi/10.1021/jacs.2c02362.

Detailed procedures for defining electronic structure-based HBs, further validation, and additional figures (PDF)

AUTHOR INFORMATION

Corresponding Author

Yousung Jung − *Department of Chemical and Biomolecular Engineering (BK21 four), Korea Advanced Institute of Science and Technology (KAIST), Daejeon 34141, South Korea;* orcid.org/0000-0003-2615-8394; Email: ysjn@kaist.ac.kr

Authors

Yonghwan Yun − *Department of Chemical and Biomolecular Engineering (BK21 four), Korea Advanced Institute of Science and Technology (KAIST), Daejeon 34141, South Korea*

Rustam Z. Khaliullin − *Department of Chemistry, McGill University, Montreal, Quebec H3A 0B8, Canada;* orcid.org/0000-0002-9073-6753

Complete contact information is available at: https://pubs.acs.org/10.1021/jacs.2c02362

Notes

The authors declare no competing financial interest.

■ ACKNOWLEDGMENTS

We are very grateful to Prof. Kyung Hwan Kim (Postech) and Prof. Jaeyoung Sung (Chung-Ang University) for helpful discussions and feedback on the manuscript, as well as to Prof. Francesco Paesani (UCSD) for providing MB-pol MD trajectories. This work was supported by National Research Foundation of Korea (NRF-2021R1A5A1030054 and 2019M3D1A1079303).

■ REFERENCES

(1) Eisenberg, D, Kauzmann, W. *The Structure and Properties of Water*; Oxford University Press: Oxford, 2005.
(2) Stillinger, F. H. Water Revisited. *Science* **1980**, *209*, 451−457.
(3) Smith, J. D.; Cappa, C. D.; Wilson, K. R.; Cohen, R. C.; Geissler, P. L.; Saykally, R. J. Unified description of temperature-dependent hydrogen-bond rearrangements in liquid water. *Proc. Natl. Acad. Sci. U.S.A.* **2005**, *102*, 14171−14174.
(4) Clark, G. N. I.; Hura, G. L.; Teixeira, J.; Soper, A. K.; Head-Gordon, T. Small-angle scattering and the structure of ambient liquid water. *Proc. Natl. Acad. Sci. U.S.A.* **2010**, *107*, 14003−14007.
(5) Kuhne, T. D.; Khaliullin, R. Z. Electronic signature of the instantaneous asymmetry in the first coordination shell of liquid water. *Nat. Commun.* **2013**, *4*, 1450.
(6) Kuhne, T. D.; Khaliullin, R. Z. Nature of the Asymmetry in the Hydrogen-Bond Networks of Hexagonal Ice and Liquid Water. *J. Am. Chem. Soc.* **2014**, *136*, 3395−3399.
(7) Niskanen, J.; Fondell, M.; Sahle, C. J.; Eckert, S.; Jay, R. M.; Gilmore, K.; Pietzsch, A.; Dantz, M.; Lu, X. Y.; McNally, D. E.; Schmitt, T.; da Cruz, V. V.; Kimberg, V.; Gel'mukhanov, F.; Fohlisch, A. Compatibility of quantitative X-ray spectroscopy with continuous distribution models of water at ambient conditions. *Proc. Natl. Acad. Sci. U.S.A.* **2019**, *116*, 4058−4063.
(8) Debenedetti, P. G. Supercooled and glassy water. *J. Phys. Condens. Mattter* **2003**, *15*, R1669−R1726.
(9) Nilsson, A.; Pettersson, L. G. M. The structural origin of anomalous properties of liquid water. *Nat. Commun.* **2015**, *6*, 8998.
(10) Poole, P. H.; Sciortino, F.; Essmann, U.; Stanley, H. E. Phase-Behavior of Metastable Water. *Nature* **1992**, *360*, 324−328.
(11) Stokely, K.; Mazza, M. G.; Stanley, H. E.; Franzese, G. Effect of hydrogen bond cooperativity on the behavior of water. *Proc. Natl. Acad. Sci. U.S.A.* **2010**, *107*, 1301−1306.
(12) Taschin, A.; Bartolini, P.; Eramo, R.; Righini, R.; Torre, R. Evidence of two distinct local structures of water from ambient to supercooled conditions. *Nat. Commun.* **2013**, *4*, 2401.
(13) Gallo, P.; Amann-Winkel, K.; Angell, C. A.; Anisimov, M. A.; Caupin, F.; Chakravarty, C.; Lascaris, E.; Loerting, T.; Panagiotopoulos, A. Z.; Russo, J.; Sellberg, J. A.; Stanley, H. E.; Tanaka, H.; Vega, C.; Xu, L. M.; Pettersson, L. G. M. Water: A Tale of Two Liquids. *Chem. Rev.* **2016**, *116*, 7463−7500.
(14) Kim, K. H.; Spah, A.; Pathak, H.; Perakis, F.; Mariedahl, D.; Amann-Winkel, K.; Sellberg, J. A.; Lee, J. H.; Kim, S.; Park, J.; Nam, K. H.; Katayama, T.; Nilsson, A. Maxima in the thermodynamic response and correlation functions of deeply supercooled water. *Science* **2017**, *358*, 1589−1593.
(15) Palmer, J. C.; Poole, P. H.; Sciortino, F.; Debenedetti, P. G. Advances in Computational Studies of the Liquid-Liquid Transition in Water and Water-Like Models. *Chem. Rev.* **2018**, *118*, 9129−9151.
(16) Woutersen, S.; Ensing, B.; Hilbers, M.; Zhao, Z. F.; Angell, C. A. A liquid-liquid transition in supercooled aqueous solution related to the HDA-LDA transition. *Science* **2018**, *359* (6380), 1127−1130.
(17) Debenedetti, P. G.; Sciortino, F.; Zerze, G. H. Second critical point in two realistic models of water. *Science* **2020**, *369*, 289−292.
(18) Kim, K. H.; Amann-Winkel, K.; Giovambattista, N.; Spah, A.; Perakis, F.; Pathak, H.; Parada, M. L.; Yang, C.; Mariedahl, D.; Eklund, T.; Lane, T. J.; You, S.; Jeong, S.; Weston, M.; Lee, J. H.; Eom, I.; Kim, M.; Park, J.; Chun, S. H.; Poole, P. H.; Nilsson, A. Experimental observation of the liquid-liquid transition in bulk supercooled water under pressure. *Science* **2020**, *370*, 978−982.
(19) Kringle, L.; Thornley, W. A.; Kay, B. D.; Kimmel, G. A. Reversible structural transformations in supercooled liquid water from 135 to 245 K. *Science* **2020**, *369*, 1490−1492.
(20) Huang, C.; Wikfeldt, K. T.; Tokushima, T.; Nordlund, D.; Harada, Y.; Bergmann, U.; Niebuhr, M.; Weiss, T. M.; Horikawa, Y.; Leetmaa, M.; Ljungberg, M. P.; Takahashi, O.; Lenz, A.; Ojamae, L.; Lyubartsev, A. P.; Shin, S.; Pettersson, L. G. M.; Nilsson, A. The inhomogeneous structure of water at ambient conditions. *Proc. Natl. Acad. Sci. U.S.A.* **2009**, *106*, 15214−15218.
(21) Soper, A. K.; Teixeira, J.; Head-Gordon, T. Is ambient water inhomogeneous on the nanometer-length scale? *Proc. Natl. Acad. Sci. U.S.A.* **2010**, *107*, E44−E44.
(22) Huang, C.; Wikfeldt, K. T.; Tokushima, T.; Nordlund, D.; Harada, Y.; Bergmann, U.; Niebuhr, M.; Weiss, T. M.; Horikawa, Y.; Leetmaa, M.; Ljungberg, M. P.; Takahashi, O.; Lenz, A.; Ojamae, L.; Lyubartsev, A. P.; Shin, S.; Pettersson, L. G. M.; Nilsson, A. Reply to Soper et al.: Fluctuations in water around a bimodal distribution of local hydrogen-bonded structural motifs. *Proc. Natl. Acad. Sci. U.S.A.* **2010**, *107*, E45−E45.
(23) Naserifar, S.; Goddard, W. A. Liquid water is a dynamic polydisperse branched polymer. *Proc. Natl. Acad. Sci. U.S.A.* **2019**, *116*, 1998−2003.
(24) Head-Gordon, T.; Paesani, F. Water is not a dynamic polydisperse branched polymer. *Proc. Natl. Acad. Sci. U.S.A.* **2019**, *116*, 13169−13170.
(25) Ohmine, I. Liquid Water Dynamics - Collective Motions, Fluctuation, and Relaxation. *J. Phys. Chem.* **1995**, *99*, 6767−6776.
(26) Elrod, M. J.; Saykally, R. J. Many-Body Effects in Intermolecular Forces. *Chem. Rev.* **1994**, *94*, 1975−1997.
(27) Ludwig, R. Water: From clusters to the bulk. *Angew. Chem., Int. Ed.* **2001**, *40*, 1808−1827.
(28) Ojamae, L.; Hermansson, K. Ab-Initio Study of Cooperativity in Water Chains - Binding-Energies and Anharmonic Frequencies. *J. Phys. Chem.* **1994**, *98*, 4271−4282.
(29) Xantheas, S. S. Cooperativity and hydrogen bonding network in water clusters. *Chem. Phys.* **2000**, *258*, 225−231.
(30) Glendening, E. D. Natural energy decomposition analysis: Extension to density functional methods and analysis of cooperative effects in water clusters. *J. Phys. Chem. A* **2005**, *109*, 11936−11940.
(31) Cobar, E. A.; Horn, P. R.; Bergman, R. G.; Head-Gordon, M. Examination of the hydrogen-bonding networks in small water clusters (n = 2−5, 13, 17) using absolutely localized molecular orbital energy decomposition analysis. *Phys. Chem. Chem. Phys.* **2012**, *14*, 15328−15339.
(32) Stone, A. J. *The Theory of Intermolecular Forces*, 2nd ed.; Oxford University Press: Oxford, 2013.
(33) Perez, C.; Zaleski, D. P.; Seifert, N. A.; Temelso, B.; Shields, G. C.; Kisiel, Z.; Pate, B. H. Hydrogen Bond Cooperativity and the Three-Dimensional Structures of Water Nonamers and Decamers. *Angew. Chem., Int. Ed.* **2014**, *53*, 14368−14372.
(34) Kananenka, A. A.; Skinner, J. L. Unusually strong hydrogen bond cooperativity in particular $(H_2O)_{(20)}$ clusters. *Phys. Chem. Chem. Phys.* **2020**, *22*, 18124−18131.
(35) Khaliullin, R. Z.; Cobar, E. A.; Lochan, R. C.; Bell, A. T.; Head-Gordon, M. Unravelling the origin of intermolecular interactions using absolutely localized molecular orbitals. *J. Phys. Chem. A* **2007**, *111*, 8753−8765.
(36) Marzari, N.; Mostofi, A. A.; Yates, J. R.; Souza, I.; Vanderbilt, D. Maximally localized Wannier functions: Theory and applications. *Rev. Mod. Phys.* **2012**, *84*, 1419.
(37) Luzar, A.; Chandler, D. Hydrogen-bond kinetics in liquid water. *Nature* **1996**, *379*, 55−57.
(38) Wernet, P.; Nordlund, D.; Bergmann, U.; Cavalleri, M.; Odelius, M.; Ogasawara, H.; Naslund, L. A.; Hirsch, T. K.; Ojamae, L.; Glatzel, P.; Pettersson, L. G. M.; Nilsson, A. The structure of the first coordination shell in liquid water. *Science* **2004**, *304*, 995−999.
(39) Kuo, I. F. W.; Mundy, C. J. An ab initio molecular dynamics study of the aqueous liquid-vapor interface. *Science* **2004**, *303*, 658−660.

https://doi.org/10.1021/jacs.2c02362
J. Am. Chem. Soc. 2022, 144, 13127−13136

(40) Sellberg, J. A.; Huang, C.; McQueen, T. A.; Loh, N. D.; Laksmono, H.; Schlesinger, D.; Sierra, R. G.; Nordlund, D.; Hampton, C. Y.; Starodub, D.; DePonte, D. P.; Beye, M.; Chen, C.; Martin, A. V.; Barty, A.; Wikfeldt, K. T.; Weiss, T. M.; Caronna, C.; Feldkamp, J.; Skinner, L. B.; Seibert, M. M.; Messerschmidt, M.; Williams, G. J.; Boutet, S.; Pettersson, L. G.; Bogan, M. J.; Nilsson, A. Ultrafast X-ray probing of water structure below the homogeneous ice nucleation temperature. *Nature* **2014**, *510*, 381−384.
(41) Reddy, S. K.; Moberg, D. R.; Straight, S. C.; Paesani, F. Temperature-dependent vibrational spectra and structure of liquid water from classical and quantum simulations with the MB-pol potential energy function. *J. Chem. Phys.* **2017**, *147*, 244504.
(42) Morawietz, T.; Urbina, A. S.; Wise, P. K.; Wu, X. E.; Lu, W. J.; Ben-Amotz, D.; Markland, T. E. Hiding in the Crowd: Spectral Signatures of Overcoordinated Hydrogen-Bond Environments. *J. Phys. Chem. Lett.* **2019**, *10*, 6067−6073.
(43) Ansari, N.; Onat, B.; Sosso, G. C.; Hassanali, A. Insights into the Emerging Networks of Voids in Simulated Supercooled Water. *J. Phys. Chem. B* **2020**, *124*, 2180−2190.
(44) Sun, Q. Local statistical interpretation for water structure. *Chem. Phys. Lett.* **2013**, *568*, 90−94.
(45) Shiratani, E.; Sasai, M. Growth and collapse of structural patterns in the hydrogen bond network in liquid water. *J. Chem. Phys.* **1996**, *104*, 7671−7680.
(46) Shiratani, E.; Sasai, M. Molecular scale precursor of the liquid-liquid phase transition of water. *J. Chem. Phys.* **1998**, *108*, 3264−3276.
(47) Wikfeldt, K. T.; Nilsson, A.; Pettersson, L. G. M. Spatially inhomogeneous bimodal inherent structure of simulated liquid water. *Phys. Chem. Chem. Phys.* **2011**, *13*, 19918−19924.
(48) Santra, B.; DiStasio, R. A.; Martelli, F.; Car, R. Local structure analysis in ab initio liquid water. *Mol. Phys.* **2015**, *113*, 2829−2841.
(49) Silvestrelli, P. L.; Parrinello, M. Water molecule dipole in the gas and in the liquid phase. *Phys. Rev. Lett.* **1999**, *82*, 3308−3311.
(50) Reddy, S. K.; Straight, S. C.; Bajaj, P.; Pham, C. H.; Riera, M.; Moberg, D. R.; Morales, M. A.; Knight, C.; Gotz, A. W.; Paesani, F. On the accuracy of the MB-pol many-body potential for water: Interaction energies, vibrational frequencies, and classical thermodynamic and dynamical properties from clusters to liquid water and ice. *J. Chem. Phys.* **2016**, *145*, 194504.
(51) Berendsen, H. J. C.; Grigera, J. R.; Straatsma, T. P. The Missing Term in Effective Pair Potentials. *J. Chem. Phys.* **1987**, *91*, 6269−6271.
(52) Abascal, J. L. F.; Vega, C. A general purpose model for the condensed phases of water: TIP4P/2005. *J. Chem. Phys.* **2005**, *123*, 234505.
(53) Cisneros, G. A.; Wikfeldt, K. T.; Ojamae, L.; Lu, J. B.; Xu, Y.; Torabifard, H.; Bartok, A. P.; Csanyi, G.; Molinero, V.; Paesani, F. Modeling Molecular Interactions in Water: From Pairwise to Many Body Potential Energy Functions. *Chem. Rev.* **2016**, *116*, 7501−7528.
(54) Bussi, G.; Donadio, D.; Parrinello, M. Canonical sampling through velocity rescaling. *J. Chem. Phys.* **2007**, *126*, 014101.
(55) Kuhne, T. D.; Iannuzzi, M.; Del Ben, M.; Rybkin, V. V.; Seewald, P.; Stein, F.; Laino, T.; Khaliullin, R. Z.; Schutt, O.; Schiffmann, F.; Golze, D.; Wilhelm, J.; Chulkov, S.; Bani-Hashemian, M. H.; Weber, V.; Borstnik, U.; Taillefumier, M.; Jakobovits, A. S.; Lazzaro, A.; Pabst, H.; Muller, T.; Schade, R.; Guidon, M.; Andermatt, S.; Holmberg, N.; Schenter, G. K.; Hehn, A.; Bussy, A.; Belleflamme, F.; Tabacchi, G.; Gloss, A.; Lass, M.; Bethune, I.; Mundy, C. J.; Plessl, C.; Watkins, M.; VandeVondele, J.; Krack, M.; Hutter, J. CP2K: An electronic structure and molecular dynamics software package - Quickstep: Efficient and accurate electronic structure calculations. *J. Chem. Phys.* **2020**, *152*, 194103.
(56) VandeVondele, J.; Hutter, J. Gaussian basis sets for accurate calculations on molecular systems in gas and condensed phases. *J. Chem. Phys.* **2007**, *127*, 114105.
(57) Goedecker, S.; Teter, M.; Hutter, J. Separable dual-space Gaussian pseudopotentials. *Phys. Rev. B* **1996**, *54*, 1703−1710.
(58) Krack, M. Pseudopotentials for H to Kr optimized for gradient-corrected exchange-correlation functionals. *Theor. Chem. Acc.* **2005**, *114*, 145−152.
(59) Becke, A. D. Density-Functional Exchange-Energy Approximation with Correct Asymptotic-Behavior. *Phys. Rev. A* **1988**, *38*, 3098−3100.
(60) Lee, C. T.; Yang, W. T.; Parr, R. G. Development of the Colle-Salvetti Correlation-Energy Formula into a Functional of the Electron-Density. *Phys. Rev. B* **1988**, *37*, 785−789.
(61) Grimme, S.; Antony, J.; Ehrlich, S.; Krieg, H. A consistent and accurate ab initio parametrization of density functional dispersion correction (DFT-D) for the 94 elements H-Pu. *J. Chem. Phys.* **2010**, *132*, 154104.
(62) Lenz, A.; Ojamae, L. Theoretical IR spectra for water clusters $(H_2O)(n)$ (n = 6−22, 28, 30) and identification of spectral contributions from different H-bond conformations in gaseous and liquid water. *J. Phys. Chem. A* **2006**, *110*, 13388−13393.
(63) Ramos-Cordoba, E.; Lambrecht, D. S.; Head-Gordon, M. Charge-transfer and the hydrogen bond: Spectroscopic and structural implications from electronic structure calculations. *Faraday Discuss.* **2011**, *150*, 345−362.
(64) Zhang, C.; Khaliullin, R. Z.; Bovi, D.; Guidoni, L.; Kuhne, T. D. Vibrational Signature of Water Molecules in Asymmetric Hydrogen Bonding Environments. *J. Phys. Chem. Lett.* **2013**, *4*, 3245−3250.
(65) Elgabarty, H.; Khaliullin, R. Z.; Kuhne, T. D. Covalency of hydrogen bonds in liquid water can be probed by proton nuclear magnetic resonance experiments. *Nat. Commun.* **2015**, *6*, 8318.
(66) Fransson, T.; Harada, Y.; Kosugi, N.; Besley, N. A.; Winter, B.; Rehr, J. J.; Pettersson, L. G. M.; Nilsson, A. X-ray and Electron Spectroscopy of Water. *Chem. Rev.* **2016**, *116*, 7551−7569.
(67) Shi, Y. F.; Scheiber, H.; Khaliullin, R. Z. Contribution of the Covalent Component of the Hydrogen-Bond Network to the Properties of Liquid Water. *J. Phys. Chem. A* **2018**, *122*, 7482−7490.
(68) Yun, Y.; Khaliullin, R. Z.; Jung, Y. Low-Dimensional Confined Ice Has the Electronic Signature of Liquid Water. *J. Phys. Chem. Lett.* **2019**, *10*, 2008−2016.

https://doi.org/10.1021/jacs.2c02362
J. Am. Chem. Soc. 2022, 144, 13127−13136